# BER analysis of 2PSK, 4PSK, and 16QAM with decision feedback channel estimation in frequency-selective slow Rayleigh fading



doi: 10.1109/25.790531

# BER Analysis of 2PSK, 4PSK, and 16QAM with Decision Feedback Channel Estimation in Frequency-Selective Slow Rayleigh Fading

Fumiyuki Adachi, *Senior Member, IEEE*

***Abstract*— The average bit error rate (BER) performances of coherently detected 2PSK, 4PSK, and 16QAM in frequency-selective slow Rayleigh fading are analyzed. Decision feedback channel estimation (DFCE) is considered, in which the past $L$-received signal samples are remodulated to remove the modulation phase by feeding back the detected symbol sequence and then averaged. Analytical expressions for the conditional BER for the given transmitted symbol sequence are derived, and the average BER performances are evaluated by Monte Carlo simulation. It is shown that as $L$ increases, the BER performance improves and approaches that of ideal coherent detection (with perfect channel estimation), and the loss in $E_b/N_0$ required for BER $= 0.1\%$ relative to ideal coherent detection becomes as small as 0.4 dB when $L = 10$. It is found that while the best performance is achieved by 2PSK and 4PSK when additive white Gaussian noise (AWGN) is the predominant cause of error (i.e., low $E_b/N_0$ regions), 16QAM modulation can achieve almost the same performance as 4PSK when the delay spread is the predominant cause of error (i.e., large $E_b/N_0$ regions), and the worst performance in this case is by 2PSK. The effects of power delay profile shape (double-spike, exponential, and Gaussian profiles assumed), rolloff factors of the Nyquist transmit/receive filters, and the transmitted symbol sequence pattern on the average BER performance are discussed.**

***Index Terms*— Channel estimation, frequency-selective, PSK, QAM, Rayleigh fading.**

## I. Introduction

MOBILE radio systems require highly bandwidth-efficient digital modulation schemes because of the limited resources of the available radio spectrum. Recently, 16-level modulation schemes, e.g., 16-square quadrature amplitude modulation (QAM) and 16-star QAM [or sometimes called differentially encoded 16-level amplitude/phase shift keying (16DAPSK)], are being intensively studied [1]. In mobile systems, the transmitted signal is reflected by many obstacles, e.g., buildings, and thus received via many propagation paths with different time delays [2]. This produces time- and frequency-selective multipath fading. Frequency-selective fading places a upper limit on the maximum allowable transmission bit rate. Although differentially encoded and detected 16-star QAM has been extensively analyzed both in frequency-nonselective fading channels [3]–[6] and in frequency-selective fading channels [7], [8], most of the literature on 16-square QAM performance has been devoted to frequency-nonselective fading channels [1, ch. 10], [3], [9]. There have been few reports dealing with frequency-selective fading channels for 16-square QAM [10], and [10] has shown by computer simulation that 16-square QAM can provide almost the same irreducible bit error rate (BER) due to delay spread as 4PSK. However, there has been no theoretical analysis of 16-square QAM in frequency-selective fading channels.

This paper theoretically analyzes 16-square QAM in frequency-selective slow Rayleigh fading channels (hereafter we use the term 16QAM for simplicity). Slow fading implies that the effect of time-selective fading can be neglected so that transmission errors are mainly produced by intersymbol interference (ISI) due to the frequency selectivity of the multipath channel and the additive white Gaussian noise (AWGN). Coherent detection requires channel estimation to extract the phase reference. We apply decision feedback channel estimation (DFCE). The BER performance of QAM with DFCE was analyzed for AWGN channels in [11] and MPSK with DFCE for both AWGN and frequency-nonselective Rayleigh fading channels in [12] and [13]. The DFCE technique can also be applied to the differential detection of MPSK signals [14]–[17] and 16-star QAM [4], [18]. In this paper, after introducing the transmission model used in our analysis in Section II, DFCE is described and the statistical properties of the channel estimate are presented in Section III. Section IV derives the conditional BER expressions for 2PSK, 4PSK, and 16QAM for the given symbol sequence in frequency-selective slow Rayleigh fading channels. In Section V, the average BER performance is evaluated by performing a Monte Carlo simulation using the derived conditional BER expressions, and the effects of AWGN and multipath channel delay spread on the average BER performance are discussed. Also discussed in Section V are the effects of power delay profile shape (double-spike, exponential, and Gaussian profiles assumed), rolloff factors of the Nyquist transmit/receive filters, and the transmitted symbol sequence.

Manuscript received February 14, 1997; revised September 9, 1997.

The author is with the Wireless Laboratories, NTT Mobile Communications Network, Inc., Kanagawa-ken 239-8536, Japan (e-mail: adachi@mlab.yrp.nttdocomo.co.jp).

Publisher Item Identifier S 0018-9545(99)05740-0.

## II. Transmission Model

The transmission model is shown in Fig. 1. The 2PSK, 4PSK, and 16QAM signals to be transmitted can be repre-

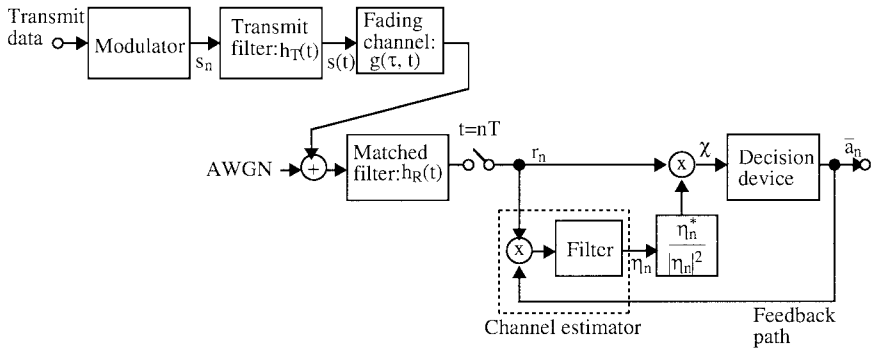


Fig. 1. Transmission model.

sented in the complex form as

$$s(t) = \sum_{n=-\infty}^{\infty} s_n h_T(t-nT) = \sqrt{2\frac{E_s}{T}} \sum_{n=-\infty}^{\infty} a_n h_T(t-nT) \quad (1)$$

where $E_s$ is the average signal energy per symbol, $T$ is the symbol duration, and $h_T(t)$ is the transmit filter impulse response. The average of $|a_n|^2$ is normalized to unity. The signal constellations for 2PSK, 4PSK, and 16QAM modulations are illustrated in Fig. 2. The signal point in the complex form is represented by $a_n = I + jQ$, where $I$ and $Q$ denote the inphase and quadrature components of the carrier, respectively. The bit mapping into each signal point is indicated in Fig. 2. For 16QAM modulation, the $I(Q)$ component of the carrier is amplitude modulated according to the two bits $ab(cd) = 11$, 10, 00, and 01 and takes values from $\{\pm 1/\sqrt{10}, \pm 3/\sqrt{10}\}$.

The transmitted signal is received via a frequency-selective slow fading channel. We assume a wide-sense stationary uncorrelated scattering (WSSUS) channel [19]. Let $g(\tau, t)$ be the multipath channel impulse response at time $t$. For a WSSUS channel, the contributions from different scatterers creating propagation paths having different time delays are uncorrelated and the delay-time correlation function of the channel is given by

$$E[g(\tau, t+\eta)g^*(\lambda, t)] = \xi(\tau, \eta)\delta(\tau - \lambda) \quad (2)$$

where $E[.]$ denotes the ensemble average and $\delta(x)$ is the delta function. We are interested in the slow fading case only, in which we can assume $\xi(\tau, \eta) \approx \xi(\tau, 0)$ over the observation period of DFCE, where $\xi(\tau, 0)$ is called the power delay profile. Note that the time delay $\tau$ is expressed relative to its mean time delay to which the receiver symbol timing is locked as assumed in [20]. The frequency selectivity of the channel is represented by the rms delay spread defined as [19]

$$\tau_{\text{rms}} = \sqrt{\int_{-\infty}^{\infty} (\tau - \tau_{\text{mean}})^2 \xi(\tau, 0)\, d\tau}$$
$$\tau_{\text{mean}} = \int_{-\infty}^{\infty} \tau \xi(\tau, 0)\, d\tau \quad (3)$$

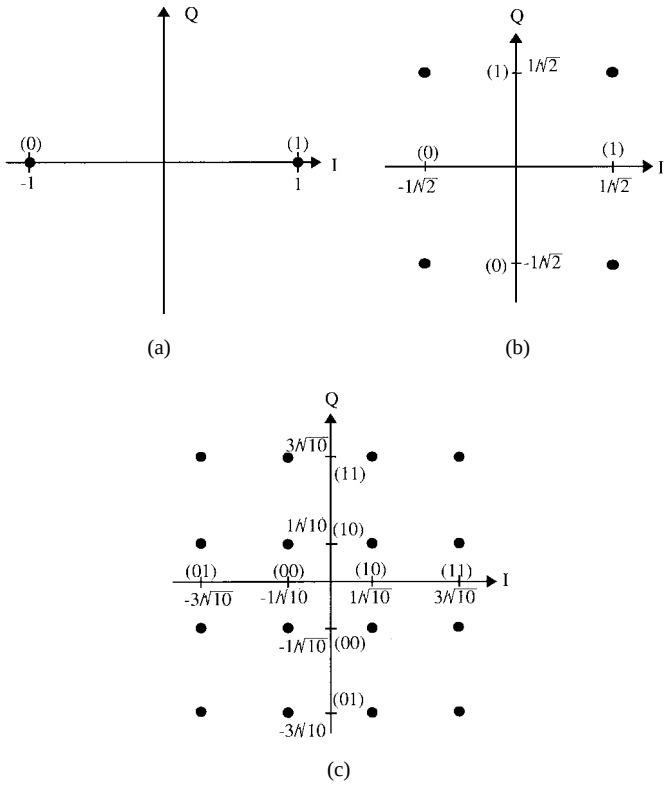


Fig. 2. Signal constellations.

where $\int_{-\infty}^{\infty} \xi(\tau, 0)\, d\tau = 1$ is assumed. As the normalized delay spread $\tau_{\text{rms}}/T$ increases, so does the ISI.

The received signal is passed through a matched filter with impulse response $h_R(t) = (1/T)h_T(-t)$ and sampled at time instant $t = nT$ for detecting the symbol $a_n$, giving

$$r_n = \sqrt{2\frac{E_s}{T}} \sum_{m=-\infty}^{\infty} a_{n-m}\, d_m + w_n \quad (4)$$

where $d_m$ is the composite channel impulse response of transmit/receive filter and multipath channel and $w_n$ is the filtered noise with zero mean and variance $= 2N_0/T$ ($N_0$ is the one-sided power spectrum density of the AWGN). Letting $h(t) = h_T \otimes h_R(t)$, where $\otimes$ denotes the convolution operation, be the overall (of the transmit/receive) filter response,

we have

$$d_m = \int_{-\infty}^{\infty} h(mT-\tau)g(\tau, t=nT)\,d\tau \tag{5}$$

where $h(0) = 1$.

## III. Decision Feedback Channel Estimation

Without loss of generality, we assume that $a_n$ is to be detected. For coherent detection, we need the phase reference at time $t = nT$. The channel estimator of Fig. 1 feeds back the past detected symbols and remodulates the received signal samples with $L$ symbols fed back to obtain the channel estimate $\eta_n$ at time $t = nT$, which is given by

$$\eta_n = \frac{\sum_{l=1}^{L} r_{n-l}\overline{a}_{n-l}^{*}}{\sum_{l=1}^{L} |\overline{a}_{n-l}|^2} \tag{6}$$

where $\overline{a}_{n-l}$ is the detected symbol at time $t = (n-l)T$ and $^*$ denotes the complex conjugate. The received signal sample $r_n$ is then divided by the channel estimate $\eta_n$ in order to remove the random amplitude and phase due to fading (the division by $\eta_n$ is equivalent to the multiplification by $\eta_n^*/|\eta_n|^2$) and to produce the decision variable $\chi$, which is given by

$$\chi = \frac{r_n}{\eta_n} = r_n\frac{\eta_n^*}{|\eta_n|^2}. \tag{7}$$

In the case of 16QAM, the two bits $ab$ are recovered from $Re[\chi]$ and the remaining two bits $cd$ recovered from $Im[\chi]$ using the decision thresholds $\delta = 0$ and $\pm 2/\sqrt{10}$, where $Re[\chi]$ and $Im[\chi]$ are, respectively, the real and imaginary parts of complex value $\chi$.

For high data rate transmission, fading can be considered to be very slow, or the fading maximum Doppler frequency (in mobile radio, given by the mobile terminal travelling speed divided by the carrier wavelength) can be, say, much less than 1% of the symbol rate $1/T$. Under such a slow fading condition, the channel impulse response can be assumed to remain almost the same over the observing period of $L$ symbols, i.e., $g(\tau, t = (n-m)T) = g(\tau, t = nT)$ for $m = 0, 1, 2, \cdots, L$. We assume here that ISI is produced from $M$ symbols in the future and $M$ symbols in the past. Substituting (4) into (6), we have

$$\begin{aligned}\eta_n &= \sqrt{2\frac{E_s}{T}}\sum_{m=-M}^{M} d_m\left(\frac{\sum_{l=1}^{L} a_{(n-l)-m}\overline{a}_{n-l}^{*}}{\sum_{l=1}^{L}|\overline{a}_{n-l}|^2}\right)\\ &\quad + \frac{\sum_{l=1}^{L} w_{n-l}\overline{a}_{n-l}^{*}}{\sum_{l=1}^{L}|\overline{a}_{n-l}|^2}\\ &= \sqrt{2\frac{E_s}{T}}\sum_{m=-M}^{M}\beta_m d_m + \vartheta\end{aligned} \tag{8}$$

where

$$\beta_m = \frac{\sum_{l=1}^{L} a_{(n-l)-m}\overline{a}_{n-l}^{*}}{\sum_{l=1}^{L}|\overline{a}_{n-l}|^2} \qquad \vartheta = \frac{\sum_{l=1}^{L} w_{n-l}\overline{a}_{n-l}^{*}}{\sum_{l=1}^{L}|\overline{a}_{n-l}|^2}. \tag{9}$$

Equation (8) can be rewritten as

$$\eta_n = \sqrt{2\frac{E_s}{T}}\beta_0 d_0 + \sum_{\substack{m=-M\\ \neq 0}}^{M}\beta_m d_m + \vartheta. \tag{10}$$

The value of $d_0$ can be expressed using the frequency responses $H(f)$ and $G(f, t = nT)$ of the transmit/receive filters and multipath channel, respectively, as

$$d_0 = \int_{-\infty}^{\infty} H(f)G(f, t=nT)\,df. \tag{11}$$

If the multipath channel frequency response is almost flat over the modulation bandwidth (or, equivalently, if the normalized delay spread $\tau_{\rm rms}/T$ is very small), we can use the approximation $G(f, t = nT) \approx G(f = 0, t = nT)$, so we obtain

$$d_0 \approx G(f=0, t=nT)\int_{-\infty}^{\infty} H(f)\,df = G(f=0, t=nT). \tag{12}$$

If no decision errors have been produced in the past, i.e., $\overline{a}_{n-l} = a_{n-l}$, we have $\beta_0 = 1$ (this approximately holds if the BER is quite small compared to the inverse of the number $L$ of fedback symbols). Consequently, in the case of small normalized delay spreads, $\eta_n$ can be used as the phase reference for coherent detection. The second and third terms in (10) are, respectively, the ISI component and the noise component. By increasing the value of $L$, the ISI and noise components decrease. However, as the normalized delay spread increases (or as the frequency selectivity of the multipath channel becomes stronger), the amplitude and phase of the channel tend to vary over the modulation bandwidth, and, thus, the estimated phase reference becomes inaccurate.

The BER analysis in Section IV involves the following three parameters:

$$\begin{aligned}\sigma_r^2 &= \tfrac{1}{2}E\left[|r_n|^2\right]\\ \sigma_\eta^2 &= \tfrac{1}{2}E\left[|\eta_n|^2\right]\\ \rho_{r\eta} &= \frac{1}{2}\frac{E[r_n\eta_n^*]}{\sigma_r\sigma_\eta}.\end{aligned} \tag{13}$$

They are given by

$$\begin{cases} \dfrac{T}{N_0}\sigma_r^2 = \dfrac{E_s}{N_0}\left[\displaystyle\sum_{m=-M}^{M} d_{m,m}|a_{n-m}|^2 + 2\sum_{m=-M}^{M} \cdot \mathrm{Re}\left[\sum_{k=-M}^{m-1} d_{m,k}\left(a_{n-m}a_{n-k}^*\right)\right]\right] + 1 \\ \dfrac{T}{N_0}\sigma_\eta^2 = \dfrac{E_s}{N_0}\left[\displaystyle\sum_{m=-M}^{M} d_{m,m}|\beta_m|^2 + 2\sum_{m=-M}^{M} \mathrm{Re}\left[\sum_{k=-M}^{m-1} d_{m,k}(\beta_m\beta_k^*)\right]\right] + \dfrac{1}{\displaystyle\sum_{l=1}^{L}|a_{n-l}|^2} \\ \dfrac{T}{N_0}\rho_{r\eta}(\sigma_r\sigma_\eta) = \dfrac{E_s}{N_0}\displaystyle\sum_{m=-M}^{M}\sum_{k=-M}^{M} d_{m,k}(a_{n-m}\beta_k^*) \end{cases} \tag{14}$$

where $\beta_m$ is defined by (9) and

$$d_{m,k} = \int_{-\infty}^{\infty} h(mT-\tau)h^*(kT-\tau)\xi(\tau, 0)\,d\tau. \tag{15}$$

## IV. BER Analysis

$W$ assume that the majority of the ISI is produced by the two immediate symbols in the future and two symbols in the past, i.e., $M = 2$ (this is valid if the delay spread $\tau_{\mathrm{rms}}$ is much smaller than the symbol length $T$). Thus, a total of $L + 5$ symbols are involved in the BER computation. We assume no decision errors in the past $L$ decisions (this assumption produces no significant error in the results for small BER regions [11]). Thus, in Rayleigh fading, given the symbol sequence, the received signal sample $r_n$ and the channel estimate $\eta_n$ become mutually correlated complex Gaussian variables.

### A. 16QAM

Since the transmitted symbols are assumed to be distributed uniformly over 16 constellation points, to obtain BER expressions for the $n$th symbol $a_n$ to be detected, it is sufficient to consider the symbols transmitted in the first quadrant only. However, we need to consider all possible sequences of the $L+4$ symbols $a_{n-l}$, $l = -2, -1, 1, 2, \cdots, L+2$. We define the following distribution functions of $\chi$:

$$\begin{cases} F_R(x) = \mathrm{Prob}[\mathrm{Re}[\chi] < x] \\ F_I(x) = \mathrm{Prob}[\mathrm{Im}[\chi] < x]. \end{cases} \tag{16}$$

Assume the transmission of $abcd = 1111$. Referring to Fig. 2, it is found that an error is produced on only the first bit $a$ if $\mathrm{Re}[\chi] < -\sqrt{2/5}$ and on only the second bit $b$ if $0 \le \mathrm{Re} < \sqrt{2/5}$ while simultaneous errors are produced on the first and second bits if $-\sqrt{2/5} \le \mathrm{Re}[\chi] < 0$. Similarly, we can find the error region of $\chi$ with respect to the last two bits $cd$. Thus, the average BER can be calculated from $P_{16\mathrm{QAM}}(1111) = 0.25[F_R(\sqrt{2/5}) + F_R(0) - F_R(-\sqrt{2/5}) + F_I(\sqrt{2/5}) + F_I(0) - F_I(-\sqrt{2/5})]$. The expressions for the average BER's of the three other transmitted 16QAM symbols, i.e., $abcd = (1110)$, $(1010)$, and $(1011)$, can be obtained similarly. The BER expressions are summarized below for the transmitted symbols in the first quadrant

$$P_{16\mathrm{QAM}}(abcd) = \begin{cases} \dfrac{1}{4}\left[F_R\left(\sqrt{\dfrac{2}{5}}\right) + F_R(0) - F_R\left(-\sqrt{\dfrac{2}{5}}\right) + F_I\left(\sqrt{\dfrac{2}{5}}\right) + F_I(0) - F_I\left(-\sqrt{\dfrac{2}{5}}\right)\right] \\ \quad \text{for } abcd = 1111 \\ \dfrac{1}{4}\left[F_R\left(\sqrt{\dfrac{2}{5}}\right) + F_R(0) - F_R\left(-\sqrt{\dfrac{2}{5}}\right) + \left\{1 - F_I\left(\sqrt{\dfrac{2}{5}}\right)\right\} + F_I(0) + F_I\left(-\sqrt{\dfrac{2}{5}}\right)\right] \\ \quad \text{for } 1110 \\ \dfrac{1}{4}\left[\left\{1 - F_R\left(\sqrt{\dfrac{2}{5}}\right)\right\} + F_R(0) + F_R\left(-\sqrt{\dfrac{2}{5}}\right) + \left\{1 - F_I\left(\sqrt{\dfrac{2}{5}}\right)\right\} + F_I(0) + F_I\left(-\sqrt{\dfrac{2}{5}}\right)\right] \\ \quad \text{for } 1010 \\ \dfrac{1}{4}\left[\left\{1 - F_R\left(\sqrt{\dfrac{2}{5}}\right)\right\} + F_R(0) + F_R\left(-\sqrt{\dfrac{2}{5}}\right) + F_I\left(\sqrt{\dfrac{2}{5}}\right) + F_I(0) - F_I\left(-\sqrt{\dfrac{2}{5}}\right)\right] \\ \quad \text{for } 1011. \end{cases} \tag{17}$$

The overall average BER given the $L+5$ symbols $a_{n-l}$, $l = -2, -1, 0, 1, \cdots, L+2$ can be obtained from

$$P_{16\mathrm{QAM}} = \frac{1}{4}\sum_{s_n(abcd)\in 1\mathrm{st\ quadrant}} P_{16\mathrm{QAM}}(abcd) \tag{18}$$

and this needs to be further averaged over all possible combinations of $a_{n-l}$, $l = -2, -1, 1, 2, \cdots, L+2$.

$F_R(x)$ and $F_I(x)$ can be derived from [21, ch. 8.2]. Using (7), (16) can be rewritten as

$$\begin{cases} F_R(x) = \mathrm{Prob}\left[\mathrm{Re}[r_n\eta_n^*] < x|\eta_n|^2\right] \\ \qquad = \mathrm{Prob}[\mathrm{Re}[(r_n - x\eta_n)\eta_n^*] < 0] \\ F_I(x) = \mathrm{Prob}\left[\mathrm{Im}[r_n\eta_n^*] < x|\eta_n|^2\right] \\ \qquad = \mathrm{Prob}\left[\mathrm{Re}[r_n - x(j\eta_n)](j\eta_n)^* < 0\right]. \end{cases} \tag{19}$$

We let

$$z_1 = \eta_n \quad z_2 = r_n - x\eta_n \tag{20}$$

to obtain

$$F_R(x) = \mathrm{Prob}[\mathrm{Re}[z_1 z_2^*] < 0]. \tag{21}$$

Noting that both $z_1$ and $z_2$ are zero-mean complex Gaussian variables, we refer to [21, pp. 320–323], and we readily obtain

$$F_R(x) = \frac{1}{2}\left[1 - \frac{\mathrm{Re}[\mu(x)]}{\sqrt{1 - \mathrm{Im}^2[\mu(x)]}}\right] \tag{22}$$

where $\mu(x)$ is the normalized cross correlation of $z_1$ and $z_2$ defined as

$$\mu(x) = \frac{\frac{1}{2}E[z_1^* z_2]}{\sqrt{\frac{1}{2}E[|z_1|^2]}\sqrt{\frac{1}{2}E[|z_2|^2]}}. \tag{23}$$

Since

$$\begin{cases} \frac{1}{2}E\big[|z_1|^2\big] = \frac{1}{2}E\big[|\eta_n|^2\big] = \sigma_\eta^2 \\ \frac{1}{2}E\big[|z_2|^2\big] = \frac{1}{2}E\big[|r_n - x\eta_n|^2\big] \\ \qquad\qquad = \sigma_r^2 + x^2\sigma_\eta^2 - 2x\sigma_r\sigma_\eta\,\mathrm{Re}[\rho_{r\eta}] \\ \frac{1}{2}E[z_1^* z_2] = \frac{1}{2}E[\eta_n^*(r_n - x\eta_n)] = \sigma_r\sigma_\eta\rho_{r\eta} - x\sigma_\eta^2 \end{cases} \tag{24}$$

we have

$$\mu(x) = \frac{\rho_{r\eta} - x\left(\frac{\sigma_\eta}{\sigma_r}\right)}{\sqrt{1 + x^2\left(\frac{\sigma_\eta}{\sigma_r}\right)^2 - 2x\left(\frac{\sigma_\eta}{\sigma_r}\right)\mathrm{Re}[\rho_{r\eta}]}}. \tag{25}$$

Replacing $\eta_n$ with $j\eta_n$ in (20), (21) gives $F_I(x)$, and, therefore, we have

$$f_I(x) = \frac{1}{2}\left[1 - \frac{\mathrm{Re}[\mu'(x)]}{\sqrt{1 - \mathrm{Im}^2[\mu'(x)]}}\right] \tag{26}$$

where

$$\mu'(x) = \frac{-j\rho_{r\eta} - x\left(\frac{\sigma_\eta}{\sigma_r}\right)}{\sqrt{1 + x^2\left(\frac{\sigma_\eta}{\sigma_r}\right)^2 - 2x\left(\frac{\sigma_\eta}{\sigma_r}\right)\mathrm{Im}[\rho_{r\eta}]}}. \tag{27}$$

Finally, by substituting (25) into (22) and (27) into (26), $F_R(x)$ and $F_I(x)$ are shown in (28), given at the bottom of the page, where $\sigma_r\sigma_\eta$ and $\rho_{r\eta}$ are given by (14).

### B. 2PSK and 4PSK

We assume $a_n = (1+j)/\sqrt{2}$ (which corresponds to the transmission of "11") for 4PSK and $a_n = 1$ (which corresponds to the transmission of "1") for 2PSK. However, note that other $L+4$ symbols can take any possible value with equal probability as assumed in the analysis of 16QAM. For 4PSK, the transmitted symbol is recovered based on the signs of the detector outputs $I$ and $Q$ while, for 2PSK, the transmitted binary symbol is recovered based on the sign of $I$ only. Therefore, the BER expressions are given by

$$\begin{cases} P_{4\mathrm{PSK}} = \frac{1}{2}[F_R(0) + F_I(0)] \\ P_{2\mathrm{PSK}} = F_R(0). \end{cases} \tag{29}$$

### C. Special Case: Frequency-Nonselective Fading

In this case, we let $\tau_{\mathrm{rms}}/T \to 0$ and $g(\tau, t) \to \delta(\tau)g(t)$. Thus, $d_m$ becomes

$$d_m = h(mT)g(t = nT) = \begin{cases} g(t = nT), & \text{if } m = 0 \\ 0, & \text{otherwise} \end{cases} \tag{30}$$

and $\beta_0 = 1$. Assuming correct decision feedback, i.e., $\overline{a}_{n-l} = a_{n-l}$, the phase reference $\eta_n$ becomes

$$\eta_n = \sqrt{2\frac{E_s}{T}}\,g(t = nT) + \vartheta \tag{31}$$

where $\vartheta$ becomes the complex Gaussian noise with variance of $2(N_0/T)\left(\sum_{l=1}^{L}|a_{n-l}|^2\right)^{-1}$. Therefore, the signal-to-noise ratio (SNR) of the phase reference for the given symbol sequence is given by

$$\Gamma = \frac{E_s}{N_0}\sum_{l=1}^{L}|a_{n-l}|^2. \tag{32}$$

In particular, for 2PSK and 4PSK with circular signal constellations, $\Gamma$ is exactly given by $\Gamma = LE_s/N_0$. Thus, one can easily understand that the SNR of the phase reference improves as $L$ increases and the BER performance may approach that of ideal coherent detection (perfect channel estimation). Referring to [3] and [22], the theoretical BER of ideal coherent detection can be expressed as a function of average $E_b/N_0$

$$\begin{cases} F_R(x) = \frac{1}{2}\left[1 - \dfrac{\mathrm{Re}[\rho_{r\eta}] - x\left(\frac{\sigma_\eta}{\sigma_r}\right)}{\sqrt{1 - \mathrm{Im}^2[\rho_{r\eta}] + x^2\left(\frac{\sigma_\eta}{\sigma_r}\right)^2 - 2x\left(\frac{\sigma_\eta}{\sigma_r}\right)\mathrm{Re}[\rho_{r\eta}]}}\right] \\ F_I(x) = \frac{1}{2}\left[1 - \dfrac{\mathrm{Im}[\rho_{r\eta}] - x\left(\frac{\sigma_\eta}{\sigma_r}\right)}{\sqrt{1 - \mathrm{Re}^2[\rho_{r\eta}] + x^2\left(\frac{\sigma_\eta}{\sigma_r}\right)^2 - 2x\left(\frac{\sigma_\eta}{\sigma_r}\right)\mathrm{Im}[\rho_{r\eta}]}}\right] \end{cases} \tag{28}$$

$(=(E_s/N_0)/\log_2 M, M = 2, 4, \text{ and } 16)$ as

$$P_{\text{ideal CD}} = \begin{cases} \dfrac{1}{2}\left[1 - \sqrt{\dfrac{\frac{E_b}{N_0}}{\frac{E_b}{N_0}+1}}\right] \\ \quad \text{for 2PSK and 4PSK} \\ \dfrac{1}{2}\left[1 - \dfrac{3}{4}\sqrt{\dfrac{4\frac{E_b}{N_0}}{4\frac{E_b}{N_0}+\frac{5}{2}}} - \dfrac{1}{2}\sqrt{\dfrac{4\frac{E_b}{N_0}}{4\frac{E_b}{N_0}+\frac{5}{18}}} + \dfrac{1}{4}\sqrt{\dfrac{4\frac{E_s}{N_0}}{4\frac{E_s}{N_0}+\frac{1}{10}}}\right] \\ \quad \text{for 16QAM.} \end{cases} \tag{33}$$

## V. Simulation Results

### A. Simulation Procedure

The average BER performances are evaluated based on the Monte Carlo simulation technique using the derived conditional average BER expressions. As in [20], we assume that the sampling timing is locked to the mean delay $\tau_{\text{mean}}$, therefore, we assume below $\tau_{\text{mean}} = 0$ without loss of generality. It is shown in [10], [20], and [23] that the BER performance is strongly affected by the delay spread, but the power delay profile shape has a negligible impact if $\tau_{\text{mean}}/T < 0.2$. For the simulation, however, we consider three types of power delay profile [20]

$$\xi(\tau, 0) = \begin{cases} \dfrac{1}{\tau_{\text{rms}}} \exp\left[-\dfrac{\tau+\tau_{\text{rms}}}{\tau_{\text{rms}}}\right], \quad \tau \geq -\tau_{\text{rms}} \\ \quad \text{for one-sided exponential} \\ \frac{1}{2}\delta(\tau+\tau_{\text{rms}}) + \frac{1}{2}\delta(\tau-\tau_{\text{rms}}) \\ \quad \text{for double-spike} \\ \dfrac{1}{\sqrt{2\pi}\,\tau_{\text{rms}}} \exp\left[-\dfrac{\tau^2}{2\tau_{\text{rms}}^2}\right] \\ \quad \text{for Gaussian.} \end{cases} \tag{34}$$

The square-root-raised cosine Nyquist filters are assumed as the transmit/receive filters. The overall filter response is given by

$$h(t) = \frac{\sin(\pi t/T)}{\pi t/T} \frac{\cos(\nu\pi t/T)}{1-(2\nu t/T)^2} \tag{35}$$

where $\nu$ is the rolloff factor. The rolloff factor is an important parameter since it controls the decay of the ISI tails that affect the BER under frequency-selective fading environments [10], [20].

In the Monte Carlo simulation, the four symbols $a_n$'s in the first quadrant were transmitted at equal probability for 16QAM while $a_n = (1+j)/\sqrt{2}$ for 4PSK and $a_n = 1$ for 2PSK. The random sequence of $L+4$ symbols $a_{n-l}$, $l = -2, -1, 1, 2, \cdots, L+2$ was generated first and then, the conditional BER given the transmitted symbol $a_n$ was computed using (17) and (28). Finally, the overall average BER was computed using (18) for 16QAM and (29) for 2PSK and 4PSK. The number of symbol sequences generated in the Monte Carlo simulation for each $a_n$ was at least 8192.

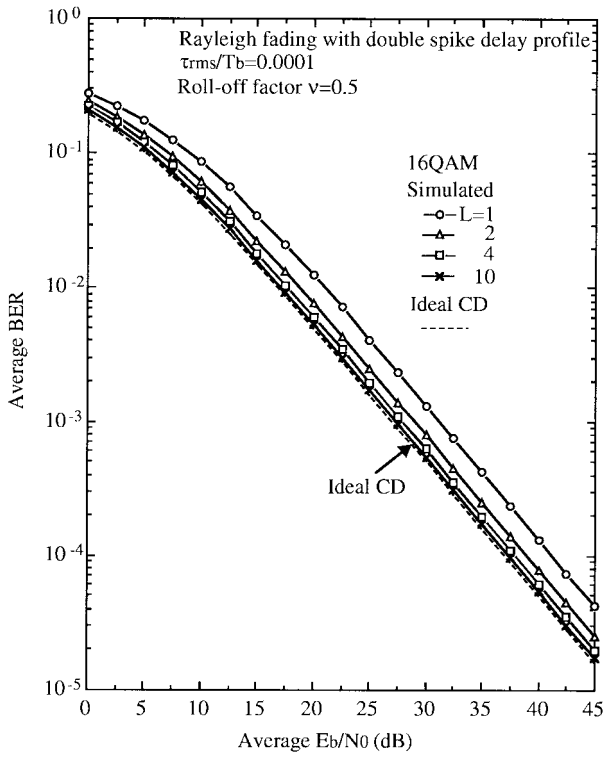


Fig. 3. BER performance of 16QAM. Double-spike delay profile with $\tau_{\text{rms}}/T_b = 0.0001$.

### B. BER Performance

The simulated average BER's of 16QAM are plotted as a function of the average SNR per bit, $E_b/N_0$ $(=0.25E_s/N_0)$, with $L$ as a parameter in Fig. 3 for a double-spike delay power profile with the normalized delay spread $\tau_{\text{rms}}/T_b = 0.0001$, where $T_b$ is the bit duration. The rolloff factor of $\nu = 0.5$ was assumed. The channel having this small normalized delay spread is viewed as a frequency-nonselective Rayleigh fading channel and the errors are mostly produced by AWGN. It is clearly seen that as $L$ increases, the SNR of the phase reference increases and the average BER performance improves. For comparison, the BER performance of ideal coherent detection (ideal CD), calculated from (33), is plotted in Fig. 3. The loss in $E_b/N_0$ required for BER $= 0.1\%$ relative to ideal $CD$ is about 2 dB when $L = 2$, but this reduces to 1 dB when $L = 4$, and the $E_b/N_0$ loss becomes as small as 0.4 dB when $L = 10$.

The BER performances of 2PSK, 4PSK, and 16 QAM modulations are compared in Fig. 4(a)–(c) for normalized delay spreads of $\tau_{\text{rms}}/T_b = 0.0001$, 0.05, and 0.2, respectively. The BER due to AWGN is exactly the same for 2PSK and 4PSK [see (33)], so only the performances of 4PSK and 16QAM are compared in Fig. 4(a) when $\tau_{\text{rms}}/T_b = 0.0001$ (where the effect of delay spread is negligible). It is clearly seen from Fig. 4(b) and (c) that when $\tau_{\text{rms}}/T_b = 0.05$ and 0.2, as the value of $E_b/N_0$ increases the BER decreases and approaches

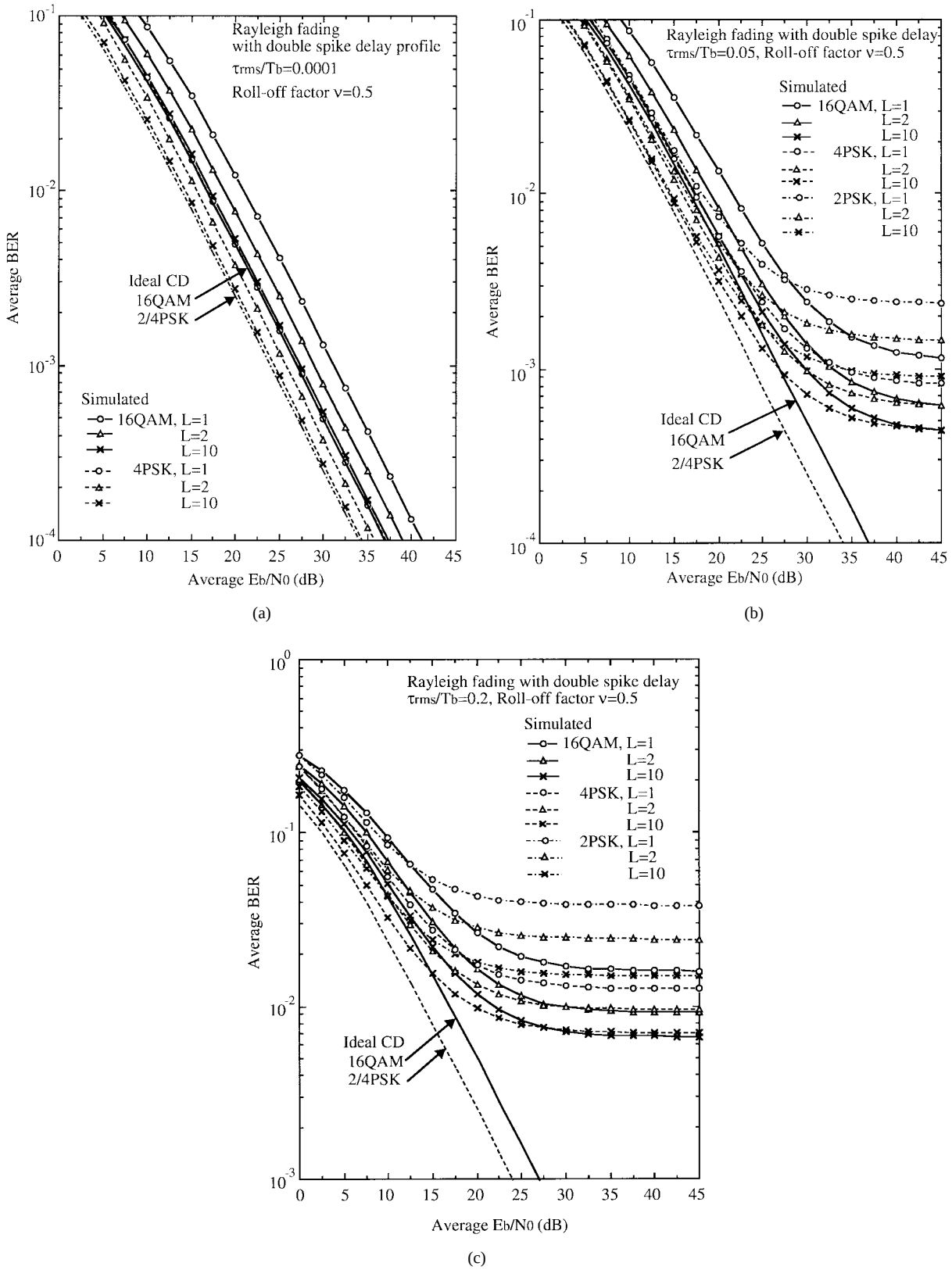


Fig. 4. Performance comparison of 2PSK, 4PSK, and 16QAM. $L = 1, 2,$ and 10. Double-spike delay profile with: (a) $\tau_{\rm rms}/T_b = 0.0001$, (b)$\tau_{\rm rms}/T_b = 0.05$, and (c) $\tau_{\rm rms}/T_b = 0.2$.

the BER floors due to the effect of delay spread (the BER floor is often called the irreducible BER due to delay spread). While the best performance is obtained by 2PSK and 4PSK, with which errors are produced by AWGN only, 16QAM provides almost the same irreducible BER's as 4PSK and the worst is produced by 2PSK. One possible reason for this is that 16QAM has symbols with three different amplitudes and the symbols with smaller amplitudes produce the smaller

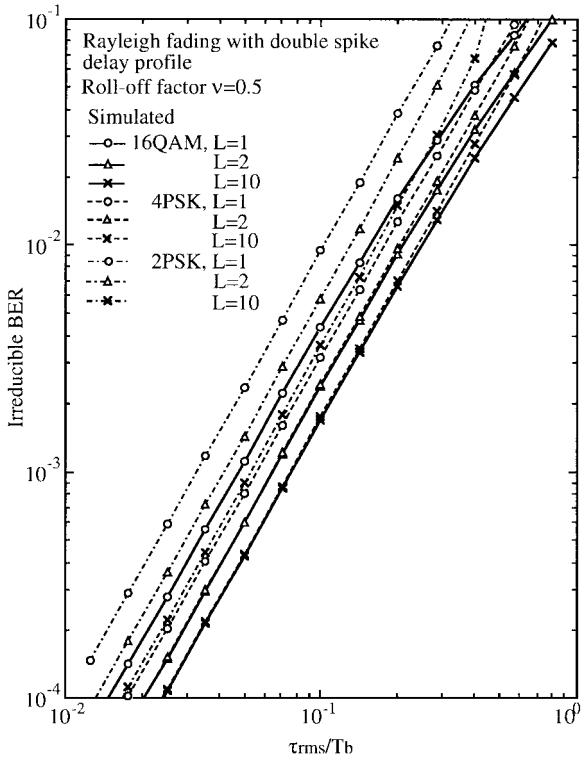


Fig. 5. Irreducible BER's of 2PSK, 4PSK, and 16QAM. Double-spike delay profile. Average $E_b/N_0 = 100$ dB.

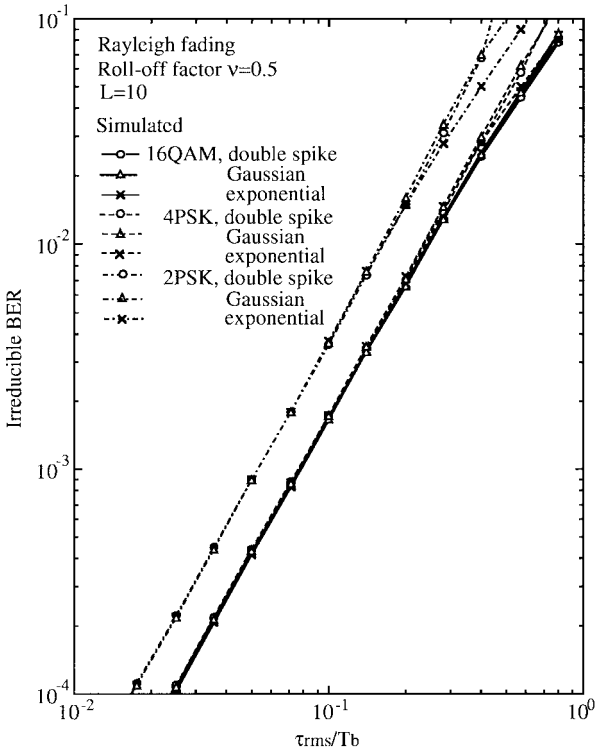


Fig. 6. Effect of delay profile shape on average BER of 2PSK, 4PSK, and 16QAM $L = 10$. Average $E_b/N_0 = 100$ dB.

ISI, contributing to the smaller irreducible BER's (this can be clearly understood from Fig. 8). On the other hand, 2PSK and 4PSK symbols have the same amplitude and always produce the same amount of ISI.

Fig. 5 plots the irreducible BER due to delay spread as a function of $\tau_{\rm rms}/T_b$ for an average $E_b/N_0$ of 100 dB and a rolloff factor of 0.5. The irreducible BER increases in proportion to the second power of $\tau_{\rm rms}/T_b$. When $\tau_{\rm rms}/T_b = 0.1$, the irreducible BER of 16QAM with $L = 10$ almost equals that of 4PSK and is about $1.7 \times 10^{-3}$ while that of 2PSK is two times larger. The simulated BER values of $\tau_{\rm rms}/T_b = 0.2$ and $\nu = 0.5$ agree quite well with those taken from [10, Fig. 4] even though the simulated BER's of [10] were gained by computer simulation using the measured delay power profile. This supports the fact found previously [20], [23] that the shape of the delay power profile has no significant impact on the irreducible BER for small normalized delay spread. The effect of the delay profile shape is shown in Fig. 6 for an average $E_b/N_0$ of 100 dB and a rolloff factor of 0.5. In the case of 16QAM, the profile shape has almost no influence on the BER performance up to $\tau_{\rm rms}/T_b = 0.8$, while in the case of 2PSK and 4PSK, the performance deviates for different profile shapes when $\tau_{\rm rms}/T_b$ becomes larger than about 0.2 and 0.4, respectively.

The effect of rolloff factor $\nu$ on the BER is shown in Fig. 7 when the average $E_b/N_0 = 20$ and 100 dB for a double-spike delay profile with $\tau_{\rm rms}/T_b = 0.05$. For an average $E_b/N_0$ of 100 dB, where most errors are produced by delay spread, the BER decreases for increasing $\nu$ because the tails of the overall filter impulse response shapes decay more quickly and the ISI decreases more. However, when we have an average $E_b/N_0$ of 20 dB, where the ISI due to delay spread can be neglected compared to that of AWGN, the BER is relatively insensitive to the rolloff factor. This can be explained below assuming the double-spike delay profile. Neglecting the ISI, it can be shown from (4) and (5) that the average SNR of the receiver matched filter output at the sampling instant $t = nT$ is approximately given by $0.5[h^2(-\tau_{\rm rms}) + h^2(\tau_{\rm rms})](E_s/N_0)$. It is found for the square-root-raised cosine Nyquist transmit/receive filters given by (35) that the SNR remains almost constant over the range of $\nu = 0$ to 1 when $\tau_{\rm rms}/T_b = 0.05$, thereby resulting in the constant BER.

The SNR of the channel estimate is affected by the transmitted symbol sequence [see (6) and (32)]. The dependence of the average BER on the symbol sequence is shown in Fig. 8 for 16QAM. It is understood from (32) that if the AWGN is the predominant cause of error, the largest SNR can be obtained, thus the smallest BER, with sequences having the largest amplitude, i.e., $a_{n-l} = (3/\sqrt{10})(\pm 1 \pm j)$, $l = 1, 2, \cdots, L$. However, this may not be true for large $E_b/N_0$ regions where the delay spread is the predominant cause of error because these sequences produce the largest ISI. Other sequences were considered: the ones having the smallest amplitude, i.e., $a_{n-l} = (1/\sqrt{10})(\pm 1 \pm j)$, $l = 1, 2, \cdots, L$. As was anticipated, it is seen in Fig. 8 that the largest amplitude sequences provide the best BER performance for the small $E_b/N_0$ regions where AWGN is the predominant cause of error, while, on the contrary, it gives the worst BER performance for the large $E_b/N_0$ regions where delay spread is the predominant cause of error.

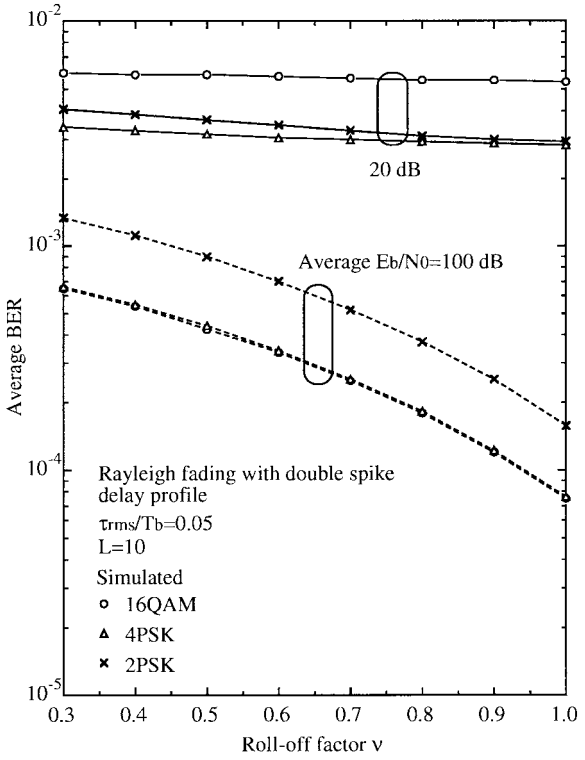


Fig. 7. Effect of filter rolloff factor on average BER of 2PSK, 4PSK, and 16QAM. Double-spike delay profile with $\tau_{\rm rms}/T_b = 0.05L = 10$.

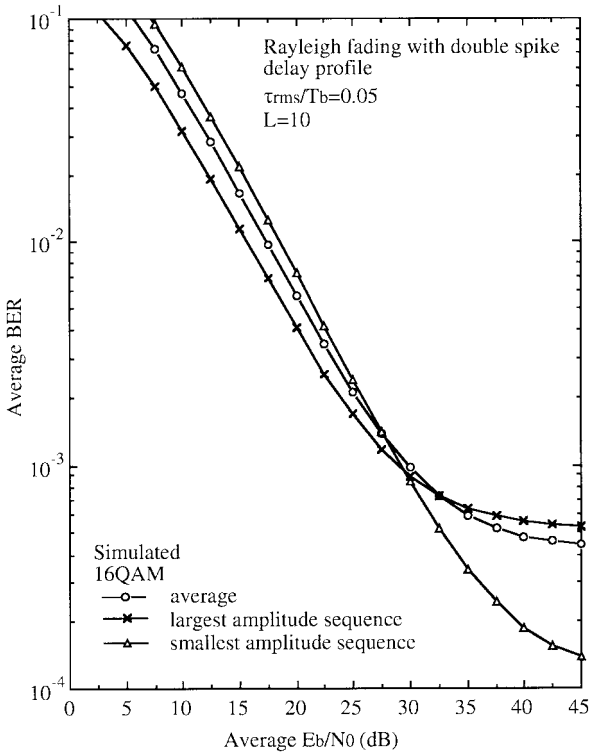


Fig. 8. Effect of transmitted sequence on average BER of 16QAM. Double-spike delay profile with $\tau_{\rm rms}/T_b = 0.05L = 10$.

## VI. Conclusion

The average BER performances of coherently detected 2PSK, 4PSK, and 16QAM with decision feedback channel estimation (DFCE) under frequency-selective slow Rayleigh fading environments were analyzed and analytical BER expressions for the given transmitted symbol sequence were derived. In the DFCE, the past $L$-received signal samples are remodulated to remove the modulation phase by feeding back the detected symbol sequence and averaged. Using the derived conditional BER expressions for the given transmitted symbol sequence, the average BER performances were obtained by Monte Carlo simulation. It was shown that the BER performance approaches that of ideal coherent detection (with perfect channel estimation) as $L$ increases and the loss in $E_b/N_0$ required for BER $= 0.1\%$ becomes as small as 0.4 dB when $L = 10$. While the best performance is achieved by 2PSK and 4PSK when the effect of AWGN is the predominant cause of error (i.e., low $E_b/N_0$ regions), 16QAM modulation can achieve almost the same performance as 4PSK when the delay spread is the predominant cause of error (i.e., large $E_b/N_0$ regions), and the worst performance is by 2PSK. The irreducible BER of 16QAM due to delay spread is almost insensitive to the power delay profile shape up to $\tau_{\rm rms}/T_b = 0.8$, however, in the case of 2PSK and 4PSK, the performance deviates for different profile shapes when $\tau_{\rm rms}/T_b$ is larger than about 0.2 and 0.4, respectively. It was also shown that the largest amplitude sequence provides the best BER performance in the low $E_b/N_0$ regions where AWGN is the predominant cause of error, while, on the contrary, it gives the worst BER performance in the large $E_b/N_0$ regions where delay spread is the predominant cause of error.

## References

[1] W. T. Webb and L. Hanzo, *Modern Quadrature Amplitude Modulation: Principles and Applications for Fixed and Wireless Channels.* London, U.K.: Pentech, 1994.

[2] W. C. Jakes, Jr., Ed., *Microwave Mobile Communications* New York: Wiley, 1974.

[3] F. Adachi and M. Sawahashi, "Performance analysis of various 16 level modulation schemes under Rayleigh fading," *Electron. Lett.*, vol. 28, pp. 1579–1580, Aug. 1992.

[4] ———, "Decision feedback differential detection of differentially encoded 16APSK signals," *IEEE Trans. Commun.*, vol. 44, pp. 416–418, Apr. 1996.

[5] T. T. Tjhung, X. Dong, F. Adachi, and K. H. Tan, "On diversity reception of narrowband 16 star-QAM in fast Rician fading," *IEEE Trans. Veh. Technol.*, to be published.

[6] F. Adachi, "Error rate analysis of differentially encoded and detected 16APSK under Rician fading," *IEEE Trans. Veh. Technol.*, vol. 45, pp. 1–11, Feb. 1996.

[7] X. Dong, T. T. Tjhung, and F. Adachi, "Error probability analysis for 16 STAR-QAM in frequency selective Rician fading with diversity reception," *IEEE Trans. Veh. Technol.*, vol. 47, pp. 924–935, Aug. 1998.

[8] Y. C. Chow, A. R. Nix, and J. P. McGeehan, "Error analysis for circular 16-DAPSK in frequency-selective Rayleigh fading channels with diversity reception," *Electron. Lett.*, vol. 30, pp. 2006–2007, Nov. 1994.

[9] S. Sampei and T. Sunaga, "Rayleigh fading compensation for QAM in land mobile radio communications," *IEEE Trans. Veh. Technol.*, vol. 42, pp. 137–147, May 1993.

[10] J. C.-I. Chuang, "The effects of delay spread on 2-PSK, 4-PSK, 8-PSK and 16-QAM in a portable radio environment," *IEEE Trans. Veh. Technol.*, vol. 38, pp. 43–45, May 1989.

[11] N. Liskov and R. Curtis, "Performance of coherent phase and amplitude digital modulations with carrier recovery noise," *IEEE Trans. Commun.*, vol. COM-35, pp. 972–976, Sept. 1987.

[12] P. Y. Kam, P. Sinha, and A. M. C. Kan, "Adaptive digital coherent receiver for MPSK," *Electron. Lett.*, vol. 28, pp. 2099–2101, Oct. 1992.

[13] P. Y. Kam and S. Y. Tay, "Adaptive reception of MPSK on fading channels," *Electron. Lett.*, vol. 30, pp. 1022–1023, June 1994.

[14] J. Liu, S. C. Kwatra, and J. Kim, "An analysis of decision feedback detection of differentially encoded MPSK signals," *IEEE Trans. Veh. Technol.*, vol. 44, pp. 261–267, May 1995.
[15] H. Leib and S. Pasupathy, "The phase of a vector perturbed by Gaussian noise and differentially coherent receivers," *IEEE Trans. Inform. Theory*, vol. 34, pp. 1491–1501, Nov. 1988.
[16] F. Edbauer, "Bit error rate of binary and quaternary DPSK signals with multiple differential feedback detection," *IEEE Trans. Commun.*, vol. 40, pp. 457–460, Mar. 1992.
[17] F. Adachi and M. Sawahashi, "Decision feedback multiple-symbol differential detection for $M$-ary DPSK," *Electron. Lett.*, vol. 29, pp. 1385–1387, July 1993.
[18] ——, "Decision feedback differential detection of 16DAPSK signals," *Electron. Lett.*, vol. 29, pp. 1455–1457, Aug. 1993.
[19] P. A. Bello, "Characterization of randomly time variant linear channels," *IEEE Trans. Commun. Syst.*, vol. CS-11, pp. 360–393, Dec. 1963.
[20] F. Adachi and K. Ohno, "BER performance of QDPSK with postdetection diversity reception in mobile radio channels," *IEEE Trans. Veh. Technol.*, vol. 40, pp. 237–249, Feb. 1991.
[21] M. Schwartz, W. R. Bennett, and S. Stein, *Communication Systems and Techniques.* New York: McGraw-Hill, 1966.
[22] J. G. Proakis, *Digital Communications*, 2nd ed. New York: McGraw-Hill, 1989.
[23] B. Glance and L. J. Greenstein, "Frequency-selective fading effects in digital mobile radio with diversity combining," *IEEE Trans. Commun.*, vol. COM-31, pp. 1085–1094, Sept. 1983.

**Fumiyuki Adachi** (M'79–SM'90) graduated from Tohoku University, Japan, in 1973 and received the Dr. Eng. degree from the same university in 1984.

In 1973, he joined Nippon Telegraph and Telephone Corporation (NTT) Laboratories, Japan, and in 1992, he transferred to NTT Mobile Communications Network, Inc. At NTT, he worked on the development of a TDMA digital cellular base station transceiver. Currently, he is a Senior Executive Research Engineer at NTT Mobile Communications Network, Inc., Kanagawa-ken, Japan, and has been leading a research group for wide-band DS-CDMA mobile radio. His research interests also include bandwidth-efficient modulation/demodulation, diversity reception, and channel coding. From 1984 to 1985, he was a United Kingdom SERC Visiting Research Fellow in the Department of Electrical Engineering and Electronics, Liverpool University, Liverpool, U.K. Since 1997, he has been a Visiting Professor at the Nara Institute of Science and Technology. He has written chapters for three books: *Fundamentals of Mobile Communications*, Y. Okumura and M. Shinji, Eds. (Japan: IEICE, 1986); *Mobile Communications*, M. Shinji, Ed. (Japan: Maruzen, 1989); and *Digital Mobile Communications*, M. Kuwabara, Ed. (Japan: Kagaku Shinbun-sha, 1992).

Dr. Adachi was a corecipient of the IEEE Vehicular Technology Society Paper of the Year Award in 1980 and again in 1990. He was also a corecipient of the IEICE Paper of the Year Award in 1996 and again in 1998. He was a Secretary of the IEEE Vehicular Technology Society Tokyo Chapter from 1991 to 1994.